Available online at www.sciencedirect.com
ScienceDirect
Journal of Catalysis 247 (2007) 20–33
JOURNAL OF CATALYSIS
www.elsevier.com/locate/jcat

Density functional theory studies of methane dissociation on anode catalysts in solid-oxide fuel cells: Suggestions for coke reduction

Natasha M. Galea, Daniel Knapp, Tom Ziegler *

Department of Chemistry, University of Calgary, Calgary, AB, T2N 1N4, Canada

Received 5 September 2006; revised 19 December 2006; accepted 27 December 2006

Available online 12 February 2007

Abstract

We studied the dissociation of methane into adsorbed carbon and hydrogen atoms on various surfaces to gain insight into carbon coke formation on solid-oxide fuel cell anodes. Preferred adsorption sites and energies were calculated for CH_x ($x = 0, \ldots, 3$) and H on Ni and Cu (111) planar and (211) stepped surfaces, on Cu–Ni and Cu–Co surface alloys, and on Ni(211) surfaces with step edge sites blocked by Au- and S-promoter atoms. Transition states and kinetic barriers were calculated on Cu(111) and Cu(211) and on the S–Ni(211) surface. Our results are in excellent agreement with existing experimental and theoretical studies, suggesting that copper anodes have very low activity and high resistance to coking, and that step-blocking on the nickel surface can increase the tolerance of nickel-based anodes to carbon coke formation.

Keywords: Solid oxide fuel cells; Coking; Carbon adsorption; Methane dissociation; Nickel catalysts; Copper catalysts; Alloy catalysts; Nickel step-blocking; Reaction kinetics; Density functional theory

1. Introduction

Fuel cells [1–7] have shown considerable promise as replacements for existing power sources by producing energy in a more efficient manner with little or no polluting emissions. Fuel cells ultimately offer the production of cleaner energy in a multitude of common applications, ranging from replacing portable batteries in cellular phones to substituting for internal combustion engines in motor vehicles. Despite considerable research activity, however, the mass market commercial production of fuel cells remains many years off. All fuel cells are composed of three main sections: an anode (fuel electrode), a cathode (oxygen electrode), and an electrolyte. The electrolyte separates the cathode from the anode and acts as an ionic conductor between the two. There are several different types of fuel cells. These types can differ in terms of the fuel required, the operating temperature of the cell, and the means by which the electrolyte carries current between the electrodes. The solid oxide fuel cell (SOFC) [1–8] (see Fig. 1) is a high-temperature electrochemical device (800–1000 °C) that generates O^{2-} ions via oxygen adsorption and reduction at the cathode, migrates these ions through the electrolyte to the anode, and finally uses these ions to oxidize adsorbed hydrogen or hydrocarbon fuels. The electrons released during the oxidation reaction flow back to the cathode through an external circuit and provide electrical power. The various reactions at the anode and cathode are outlined below. At the cathode,

$$\frac{1}{2}O_2(g)_c + 2e_c^- \longleftrightarrow O_{ec}^{2-}, \tag{1}$$

where c denotes the cathode and ec denotes the cathode side of the electrolyte. At the anode,

$$H_2(g)_a + O_{ea}^{2-} \longleftrightarrow H_2O(g)_a + 2e_a^-, \tag{2}$$

$$CO(g)_a + O_{ea}^{2-} \longleftrightarrow CO_2(g)_a + 2e_a^-, \tag{3}$$

$$CH_4(g)_a + 4O_{ea}^{2-} \longleftrightarrow 2H_2O(g)_a + CO_2(g)_a + 8e_a^-, \tag{4}$$

where a denotes the anode and ea denotes the anode side of the electrolyte. Experimentally, one of the most commonly used SOFC anode materials is porous nickel yttria-stabilized-zirconia (Ni-YSZ) [1–14] coupled to an YSZ electrolyte. Within the Ni-YSZ anode, the catalytic activity and electronic conductivity are provided by the nickel, whereas the ionic conductivity and thermal expansion match with the electrolyte are

* Corresponding author.
E-mail address: ziegler@ucalgary.ca (T. Ziegler).

0021-9517/$ – see front matter
doi:10.1016/j.jcat.2006.12.021

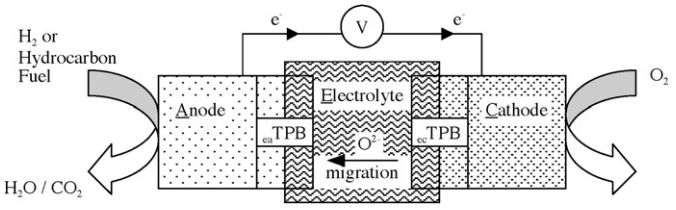

Fig. 1. Diagram of the membrane-electrode assembly (MEA) within a SOFC.

provided by the YSZ. Despite the fact that nickel has excellent catalytic activity and is a good steam-reforming catalyst, the Ni-YSZ anode composite suffers critical disadvantages. Nickel catalyzes the formation of graphitic carbon (coking) from hydrocarbon anode fuels and is intolerant to sulfur poisoning. Sulfur is found as an impurity in most hydrocarbon fuels, and its removal requires costly prepurification methods. The poisoning of the anode surface with graphitic carbon or sulfur presents a major challenge to the workings of the SOFC by blocking active adsorption sites and rendering the anode inoperable. On a nickel catalyst, the direct oxidation of hydrocarbon fuels (Eq. (4)) results in poisoning of the anode adsorption sites by the formation of graphitic carbon. When the anode fuel source is methane, this can be overcome by humidification of the fuel stream. The internal steam-reforming reaction (Eq. (5)) is able to discourage carbon formation via the formation of carbon monoxide, followed by oxidation of the resulting product gases (Eqs. (2)–(3)). For higher hydrocarbons, steam reforming does not discourage coking on the anode, due to the requirement of much higher H_2O:C ratios for stable operation. During the internal steam reforming reaction,

$$CH_4(g) + H_2O(g) \longleftrightarrow CO(g) + 3H_2(g), \tag{5}$$

both the adsorption and dissociation of water,

$$H_2O(g)_a \longleftrightarrow {}^*OH_{2a}, \tag{6}$$

$${}^*OH_{2a} \longleftrightarrow {}^*OH_a + {}^*H_a, \tag{7}$$

$${}^*OH_a \longleftrightarrow {}^*O_a + {}^*H_a, \tag{8}$$

and hydrocarbon anode fuel,

$$CH_4(g)_a \longleftrightarrow {}^*CH_{3a} + {}^*H_a, \tag{9}$$

$${}^*CH_{3a} \longleftrightarrow {}^*CH_{2a} + {}^*H_a, \tag{10}$$

$${}^*CH_{2a} \longleftrightarrow {}^*CH_a + {}^*H_a, \tag{11}$$

$${}^*CH_a \longleftrightarrow {}^*C_a + {}^*H_a, \tag{12}$$

on the anode surface as well as the formation and desorption of hydrogen molecules,

$$6{}^*H_a \longleftrightarrow 3H_2(g)_a, \tag{13}$$

and carbon monoxide,

$${}^*O_a + {}^*C_a \longleftrightarrow {}^*CO_a, \tag{14}$$

$${}^*CO_a \longleftrightarrow CO(g)_a, \tag{15}$$

occur. Using various approaches, theoretical studies of all reactions involved in the internal steam-reforming (Eq. (5)) reaction on Ni surfaces have been reported [15–21], along with calculations that consider only the adsorption and dissociation of

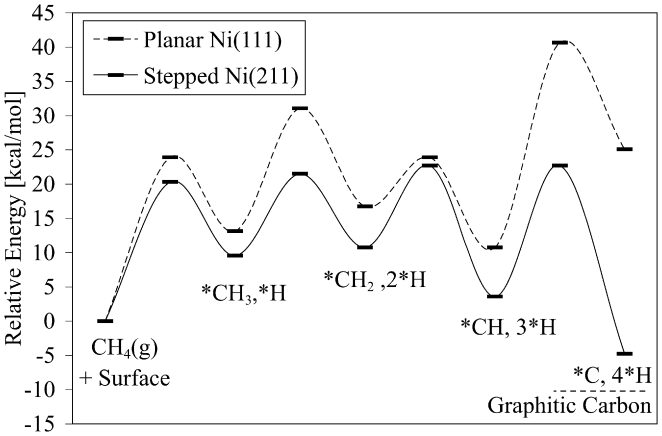

Fig. 2. Published data from Ref. [18] showing methane adsorption and dissociation on (111) planar and (211) stepped nickel surfaces.

hydrogen or methane (Eqs. (9)–(12)) [22–33]. There are two classes of active adsorption sites on a nickel surface: those associated with the planar close-packed surface and those associated with steps and defect sites. Most theoretical studies of methane adsorption and dissociation on nickel have been based on the (111) planar surface [15–20,22–33]. The general consensus is that the most thermodynamically stable adsorbate species on the nickel planar surface is *CH. Furthermore, the production of carbon, and thus also graphite, from this stable species is an endothermic process. This energy profile (shown in Fig. 2) might seem a little surprising, given the abundant formation of graphitic carbon seen experimentally on nickel anode surfaces [34–36]. The nickel planar surface data alone imply that coking should not occur on the nickel surface due to the large amount of energy required for the production of carbon. It is known, however, that the stepped surface can be far more reactive than the planar surface. This behavior has been experimentally confirmed by Dahl et al. [37], who showed that the rate of N_2 dissociation on the terraces of Ru(0001) is at least nine orders of magnitude smaller than the corresponding rate on the steps. Adsorption energy differences between the stepped and terraced surfaces also have been determined for other metals [38]. It is worth noting that whereas lower adsorption activation energies are associated with step sites, terrace sites are more abundant. The Nørskov group has published a large body of work [15–21] in which they explored the energy profile for the internal reforming reactions on both a Ni(111) planar surface and a Ni(211) stepped surface (see Fig. 2). The Nørskov group has shown that dissociation of methane on the Ni(211) surface is energetically more favorable than on the Ni(111) surface, with lower thermodynamic and kinetic energies. On the planar surface, the adsorption sites for the different species are $CH_4(g)$-onefold (1f), $^*CH_3/^*CH_2/^*CH/^*C/^*H$-threefold (3f) sites. On the corresponding stepped surface, the adsorption sites are $CH_4(g)/^*CH_3$-onefold (1f) at step edge, $^*CH_2/^*H$-twofold (2f) at the step edge, *CH/*C-fivefold (5f) site at the step base. These adsorption sites are shown in Fig. 3. Due to the limited number of adsorption sites at the steps themselves, there is a competitive relationship among the $CH_4(g)/^*CH_3$ species, the $^*CH_2/^*H$ species, and the *CH/*C species. Thermodynam-

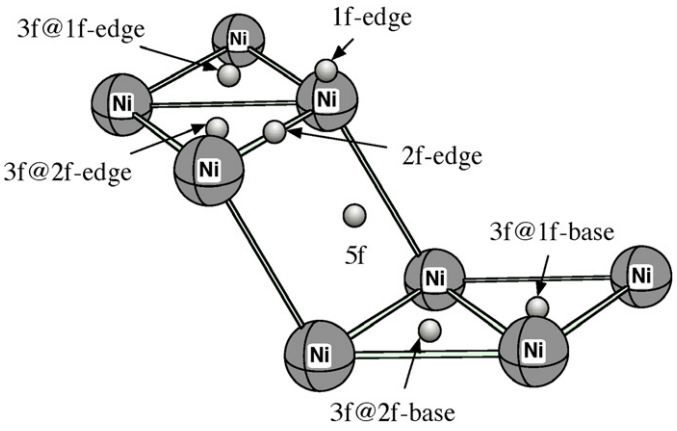

Fig. 3. Adsorption sites on the (211) stepped surface.

ically, the main difference between the two surfaces is in the production of carbon and hydrogen. This production is endothermic on the planar surface and exothermic on the stepped surface. It is this exothermic reaction on the stepped nickel surface that is the driving force for the formation of graphitic carbon, which explains experimental observations of coking on the anode surface. Further work by the Nørskov group [18,20,39] investigated the nature of the graphitic [34–36] carbon on the stepped surfaces. They demonstrated that planes of graphene grow parallel to the terrace from the base of the step, where carbon adsorption initially takes place. Graphene is thermodynamically more stable on the (111) terraces, where the nickel atoms and the hexagonally structured carbon atoms can lie parallel to one another. A finite size must be reached for the graphite island to achieve stability, and thus coke formation can be hindered by a sparse covering of promoter atoms (e.g., gold [16,18,40], sulfur [18,21,41,42], alkalis [18,43–45]). Sulfur is known as a catalyst poison [1–7]; however, small amounts of sulfur have been found to lower the production of carbon [18,21,41,42]. Theoretical calculations predict that sulfur adsorbed on a planar nickel(111) surface will occupy 3f hollow (fcc) sites, whereas on a stepped nickel(211) surface, sulfur will occupy the 5f sites at the step base [18]. The preferential adsorption of sulfur at the step has been experimentally demonstrated by scanning tunneling microscopy (STM) [42]. The Nørskov group has found that sulfur decreases the d-band center of the nickel surface, weakening the bond between methane and the surface d-electrons, and directly repels the adsorbates via Pauli repulsion, blocking methane adsorption at the step edge [21,46]. Increasing the sulfur coverage decreases the formation of coke, not only due to direct competition with carbon adsorption at the 5f step site, but also because sulfur adsorption leads to the repulsion of adsorbates at the step edge. Several research groups have used alternative anode materials to tackle coking at the anode. Such catalysts as cobalt [28,29,47], and iron (both cobalt and iron are good steam-reforming catalysts), palladium [48], platinum [49], and ruthenium [50,51], have been studied experimentally [1–8] and theoretically [28,29,47–54]. The use of these metals has not proved successful, due mainly to their propensity to catalyze carbon formation and, in some cases, their impractically high cost. Taking a different approach, some groups have replaced the nickel anode with copper [1–7,55–64]. Copper does not catalyze carbon formation, because it is a poor catalyst for C–C and C–H bond activation. One disadvantage of copper is its low melting temperature (1083 °C), which creates difficulties during the anode fabrication process [5] developed for Ni-based catalysts. Another disadvantage is that copper is a poor oxidation catalyst; a more catalytically active material must be added to the anode composite. A possible compromise is to create a copper–nickel [65–72] alloy. Gorte et al. [71,72] have published experimental studies on Cu–Ni and Cu–Co anodes demonstrating the direct oxidation of hydrocarbon fuels with little carbon formation. Alstrup et al. [68] have shown that whereas a small amount of copper (1%) can increase the rate of carbon formation in a $CO + H_2$ environment, greater amounts of copper (>10%) are detrimental to the carbon formation rate. This reduced carbon formation may be due to copper surface enrichment in Cu–Ni alloys [65–72]. Segregation of copper to the surface occurs because copper has a lower surface energy than nickel [73]. Sinfelt et al. [65] have demonstrated that a Cu–Ni catalyst containing 5% copper overall can have a 40–60% copper surface composition. Kim et al. [71] have noted that higher reduction temperatures lead to increased copper surface segregation. Many compositions of Cu–Ni alloys have been studied, and all have been shown to generate coke, although not in proportion to the percentage of nickel present [71]. It has been noted that a Cu–Ni alloy attains a melting temperature and catalytic properties at an intermediate point between the two metals [72], and that the alloy shows characteristics different from either pure nickel or copper metals. It is clear from the research reviewed above that several areas demand further scientific exploration. Given the promising experimental research carried out on copper-based catalysts [55–72], it is somewhat surprising that little theoretical research exists on the nature of copper's poor activity and resistance to coking. Despite the existence of experimental work [41–44] establishing the important effects of adding sulfur promoter atoms to the nickel surface, existing theoretical research has considered the effects of sulfur promotion only on the first step of the methane dissociation process [21,45]. In this paper, we explore in detail the dissociation of methane on Cu(111) and (211) surfaces, consider the effects of alloying copper with nickel and with cobalt, and examine the effects of promoter atoms, such as sulfur and gold, on the adsorption of methane and its derivatives on the nickel surface.

2. Computational method

Density functional theory (DFT) calculations were performed using the Vienna Ab initio Software Package (VASP) [74–77], with projector augmented wave (PAW) [78,79] potentials. All calculations were spin-polarized and conducted within the generalized gradient approximation (GGA) with the PBE exchange correlation functional [80]. The kinetic energy cutoff for all metals/surfaces was set to 25 Ry. k-Point sets were generated using the Monkhorst–Pack method [81]. Calculations on the Cu(111) surface used $5 \times 5 \times 1$ k-points in an oblique unit cell, whereas all other metals/surfaces used $4 \times 4 \times 1$ k-points in

an orthorhombic unit cell. The ideal kinetic energy and k-point cutoffs were determined by running test calculations at cutoffs of up to 37 Ry and $19 \times 19 \times 1$ k-points. Metal atoms were fixed in slab geometries at their bulk-truncated positions in an fcc lattice with experimental[1] bulk lattice constants of $a_0 = 3.52$ Å for nickel and $a_0 = 3.61$ Å for copper [82]. Relaxation of the surface layer of the slabs was found to have only a minimal effect on adsorption energies and almost no effect on the bond lengths between the adsorbates and the surface, and thus is neglected. The slabs were separated in the direction perpendicular to the surface by a vacuum region of 10 Å. Dipole interactions along this direction were found to make a negligible contribution (from 10^{-4} to 0.5 kcal/mol) to the total energy. Three layers of atoms were used in each slab, with the surface represented by a $p(2 \times 2)$ unit cell for Ni(111), Cu(111), Cu–Ni(111), and Cu–Co(111); a $p(2 \times 3)$ unit cell for Ni(211) and for Au and S on Ni(211); and a $p(3 \times 3)$ unit cell for Cu(211) and Cu on Ni(211). The three-layer slabs were tilted to create the (211) stepped geometry. Adsorbate geometries were optimized until the energy had converged to 10^{-3} eV. Some calculations (those done for the Cu(111), Cu–Ni(111), and Cu–Co(111) surfaces) used a strict force convergence criterion of 0.02 eV/Å, but the energies did not vary significantly. All transition states and reaction barriers were calculated with the nudged-elastic band method [83] used to test various reaction pathways. The improved tangent estimate [84] and climbing-image method [85] of Henkelman et al. were used to calculate the tangent to the elastic band at each point, and to search out the saddlepoint for the minimum energy path, respectively.

3. Results and discussion

3.1. Testing: Nickel surface

Dissociation of methane into its constituent carbon and hydrogen atoms on the Ni(111) surface has been extensively studied by a number of research groups. Cluster calculations have been carried out using cluster bond preparation and the complete active space self-consistent field (CASSCF) method of Siegbahn et al. [22–24], and Yang and Whitten [25–27], using the many-electron-embedding-cluster theory, to calculate the adsorption energies of CH_x ($x = 0, \ldots, 3$) and H on Ni(111). These cluster calculations show that the various adsorbates prefer to lie in the 3f position on the Ni(111) surface. Interestingly, cluster calculations carried out using density-functional theory by Burghgraef et al. [28,29] and by Au et al. [30] have shown that CH_3 is preferentially adsorbed at the onefold (1f) on-top position, whereas all other adsorbates are found to remain at the 3f position. Despite this variation in the preferred adsorption site for CH_3, and despite discrepancies among the various studies in the precise values for the adsorption energies,

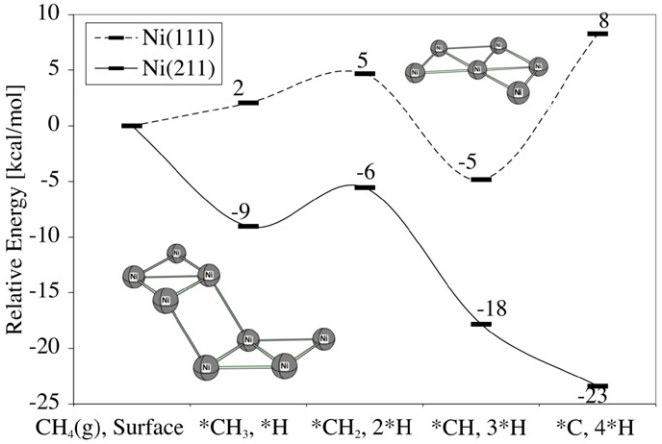

Fig. 4. Thermodynamic pathway for the dissociation of methane (CH_4) on planar (111) and stepped (211) Ni surfaces. Note that the formation of carbon is the most stable end point on the stepped surface but not on the planar surface.

all of the above investigations found the same general trend in adsorption energies: $E_{ads}(CH_3) < E_{ads}(H) < E_{ads}(CH_2) < E_{ads}(CH) < E_{ads}(C)$. Periodic slab calculations carried out using DFT by Michaelides and Hu [31–33] and Nørskov et al. [16–19] found that all adsorbates, including CH_3, lie at the 3f position. In all cases, $^*C + 4^*H$ formed the least stable intermediate, whereas $^*CH + 3^*H$ was found to be the most stable intermediate in the methane dissociation pathway. In our test calculations on the Ni(111) planar surface, the results of which are shown in Fig. 4, we obtained qualitatively equivalent results. It is important to note, however, that the thermodynamic pathway shown in Fig. 4 lies ∼10–15 kcal/mol below that reported by Bengaard et al. [18], who also used plane-wave DFT on a slab geometry. Our calculations show that this difference is almost entirely due to our use of the PBE functional [86] instead of the RPBE functional [87] adopted by Bengaard et al. [18]. This increased tendency toward exothermicity is not surprising, given that it has been argued that the PBE functional leads to overbinding of adsorbates on transition metal surfaces relative to RPBE [87]. This raises the pertinent question of why we have chosen to use the PBE functional. Kurth et al. [88] found that RPBE was better for calculating the atomization energy of some molecules but worse for others, including CH_4. Gajdos et al. [89] reported that RPBE provided more accurate adsorption energies for adsorption of CO onto various transition metal surfaces, but worse results for the noble metal surfaces Au and Ag (but not Cu). Given this potential ambiguity in the relative merits of using RPBE versus PBE in our calculations of CH_4 dissociation on various surfaces (including Au–Ni), and given that the RPBE functional currently is not fully supported within VASP (PAW potentials are not provided for RPBE), we have decided to use the PBE functional for all of our calculations. As noted above, using the PBE functional does not change the qualitative results of the calculation of methane dissociation on the Ni(111) surface, and it leads to the same conclusions arrived at in previous studies [17,18] in which the RPBE functional was used. Our test calculations of methane dissociation on the Ni(211) stepped surface, which consists of (111) terraces and (100) steps, show similar qualitative agreement with published

[1] In the case of nickel, the calculated equilibrium lattice constant was 3.52 Å, equal to the experimental value. In the case of copper, the calculated equilibrium lattice constant was 3.64 Å, a small difference of 0.8%. The thermodynamic pathway for methane dissociation was recalculated using $a_0 = 3.64$ Å for the Cu(111) surface, and the energies were found to vary by 0.5 kcal/mol.

results [18], with minor differences that are consistent with the stronger binding of adsorbates observed in our PBE-based calculations. The key point to be made here—already raised by others [18–20,36–39]—is that the Ni(211) stepped surface is more reactive than the Ni(111) planar surface and that carbon coke formation in nickel-based SOFCs can be explained by the exothermic adsorption of carbon at the step sites, followed by the formation of graphene islands covering the terraces [18,36, 39] and by the penetration of carbon into the nickel bulk [5]. In what follows, we theoretically explore a number of experimentally motivated proposals for solving the problem of coking in solid-oxide fuel cells. In particular, we study dissociation of methane on the surfaces of various anode catalyst materials and consider the possibility of step-blocking by surface alloys and promoter atoms on the Ni(211) surface.

3.2. Copper surface

Various groups have tested Ni–Cu alloys as catalysts for hydrocarbon dissociation in SOFCs [5,66–71]. It has been shown that in these systems, adding copper to the nickel catalyst greatly increases the tolerance to coking. This resistance has been attributed to the enrichment of the catalyst surface with copper, which has a lower surface energy than Ni [5,65,69,71–73]. The properties of the Ni–Cu surface have been shown to be sensitive to temperature, suggesting that formation of carbon on the surface depends strongly on the morphology of the copper and nickel on the surface [71,72]. Copper used as a catalyst alone experiences no carbon deposition, but unfortunately has poor activity [5,57,59,71,90–93]. Stable fuel cell operation has been demonstrated for Cu-ceria systems [5,57,59], in which it appears that ceria acts as the oxidation catalyst and copper acts as the anode current collector. These observations seem to be in agreement with theoretical calculations showing that dissociation of methane on the Cu(111) surface is highly endothermic [30,53,54]. Although some theoretical work has been done on the Cu(111) surface [30,53,54,92,94,95], the dissociation pathway of methane—including the kinetic barriers and transition states—has yet to be fully worked out. As of the time of this writing, we are not aware of any theoretical studies of methane dissociation on the Cu(211) surface. To elucidate the reasons for copper's poor activity in SOFC systems and for its tolerance to coking, we calculated the adsorption energies and sites, as well as the reaction barriers to dehydrogenation, of methane and its derivatives CH_x ($x = 0, \ldots, 3$) and H on both the Cu(111) planar and Cu(211) stepped surfaces.

3.2.1. Cu(111) planar surface

Adsorption energies for CH_x ($x = 0, \ldots, 3$) and H were calculated at the high-symmetry sites on the Cu(111) surface; the results are presented in Table 1, along with available data from the literature. The results presented here are in excellent agreement with other published theoretical results [30,92, 94,95], especially those calculated using plane-wave DFT in the infinite slab geometry [92,94,95]. The 3f site is found to be the preferred adsorption site for all adsorbates, with a difference in adsorption energy of 1 kcal/mol between the 3ff and 3fh sites. The adsorption energies on Cu range from 10 to 50 kcal/mol less than those on Ni. Interestingly, the adsorption energies still follow the trend $E_{ads}(CH_3) < E_{ads}(H) < E_{ads}(CH_2) < E_{ads}(CH) < E_{ads}(C)$, indicating the increasing strength of the carbon-metal bond as the CH_x fragment becomes more increasingly dehydrogenated. All transition states in the methane dissociation pathway were also calculated on the Cu(111) surface. The transition state geometries, along with those of the adsorbates at their preferred adsorption sites, are shown in Fig. 5. Methane does not freely adsorb on the copper surface in the DFT slab calculations, because it is a symmetric, closed-shell molecule. To provide an initial image for the nudged elastic band method, the height of the carbon atom was fixed, and all other degrees of freedom were optimized at the high-symmetry positions on the surface. On the Cu(111) surface, the transition state with the lowest barrier was found when CH_4 descended to the 3f position, with one of the lowest hydrogens breaking off across the twofold (2f) bridge and moving into the adjacent 3f position. The C–H bond length in the gas phase is 1.10 Å, with H–C–H bond angles of 109°. At the transition state, the C–H bond length stretches to 1.71 Å, and the reaction barrier reaches its height of 45 kcal/mol. The resulting CH_3 fragment is adsorbed onto the 3f position, 1.74 Å above the surface, with a C–H bond length of 1.11 Å and an H–C–H bond angle of 106°. All three of the hydrogen atoms point to the three nearest Cu atoms surrounding the 3f position. One of the hydrogens on the CH_3 fragment can be dissociated around a Cu atom into a far 3f position. At the transition state, the C–H bond stretches to 1.87 Å, with a reaction barrier of 33 kcal/mol. A similar dissociation pathway was found by Michaelides and Hu [94], with a reaction barrier of 31 kcal/mol. These authors also found that the transition state occurs at a C–H bond length of 1.84 Å, in excellent agreement with the results of our calculations. The adsorbed CH_2 fragment moves to within 1.4 Å of the surface, with one hydrogen atom pointing toward a copper atom (with a C–H bond length of 1.12 Å) and the other sitting across

Table 1
Adsorption energies [kcal/mol] at the high-symmetry sites on the Cu(111) surface. Differences in adsorption energies are less than 1 kcal/mol at the threefold filled (3ff) and threefold hollow (3fh) sites, with the 3fh site only slightly preferred by all adsorbates except for CH_3. The energies at the preferred adsorption sites are marked in bold

	3ff/h	2f	1f
H	**56** 49[a], 57[c]	46	35
C	**104** 86[a], 113[c]	92	60 67[c]
CH	**102** 104[a]	93	61
CH_2	**80** 69[a]	77	40
CH_3	**32** 27[a], 36[b], 34[c], 31[d]	29 34[b]	27 31[b], 30[c], 27[d]

[a] DFT cluster calculation from Au et al. [30].
[b] Plane-wave DFT results from Michaelides and Hu [94].
[c] Plane-wave DFT results from Chen et al. [95].
[d] Plane-wave DFT results from Wang et al. [92].

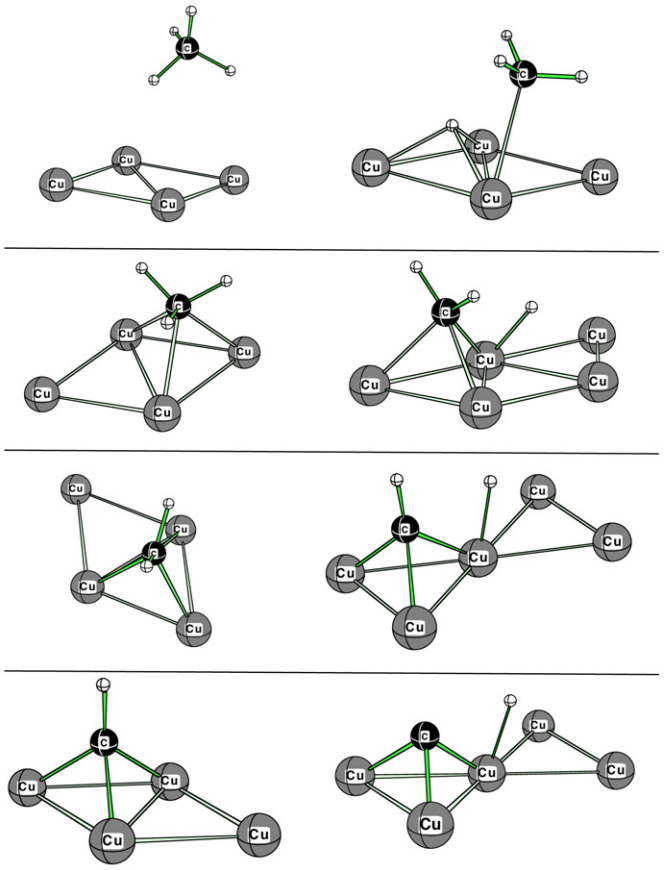

Fig. 5. Adsorption geometries of CH_x (on the left) and transition states (on the right) in the methane dissociation pathway on the Cu(111) surface.

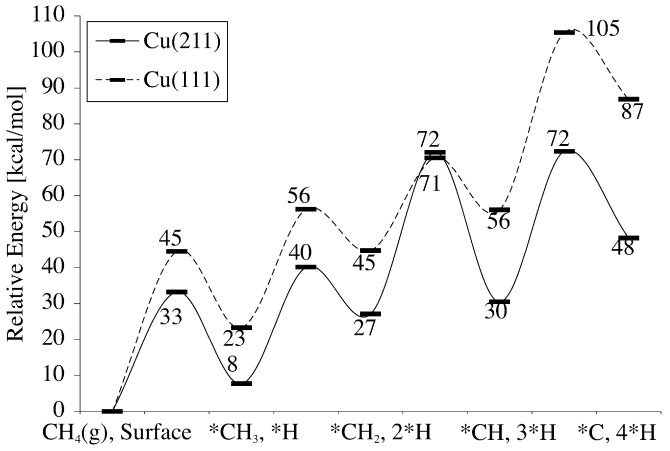

Fig. 6. Thermodynamic pathway for the dissociation of methane CH_4 on (111) planar and (211) stepped Cu surfaces. Note that all steps in the path on both surfaces are endothermic.

Table 2
Adsorption energies [kcal/mol] at the high-symmetry sites on the Cu(211) stepped surface. Energies at the preferred adsorption sites are marked in bold. Where energies are not given, the sites were not found to be stable adsorption sites

	3f@1f-edge	3f@2f-edge	1f-edge	2f-edge	5f	3f@1f-base	3f@2f-base
H	57	**60**	42	54	52	52	53
C	112	114	67	98	**134**	109	115
CH	–	115	73	100	**126**	–	–
CH_2	60	**77**	53	70	65	–	–
CH_3	30	37	35	**41**	13	–	–

the 2f bridge position (with C–H bond length of 1.11 Å). From here, the hydrogen atom closest to the Cu atom can dissociate across the Cu atom into the opposite 3f position. The barrier to this easiest step in the dissociation process is 27 kcal/mol, with the C–H bond stretching to 2.0 Å at the transition state. Adsorbed CH also finds its lowest energy at the 3f position, with the hydrogen atom pointing straight up from the surface 1.10 Å above the carbon atom. The carbon atom continues to move closer to the surface with a perpendicular separation of 1.2 Å. For the hydrogen atom to break away from the carbon atom, the CH fragment must first tilt toward one of the Cu atoms, where the hydrogen atom can dissociate across the 1f position into its favored 3f position. This last step in the methane dissociation process is also the hardest, with a reaction barrier of 49 kcal/mol. The C–H bond is stretched to 2.02 Å at the transition state. The lone carbon and hydrogen atoms settle into the 3f positions, with C experiencing a much stronger interaction with the surface than H, as can be seen from their adsorption energies given in Table 1. The H atom lies 0.93 Å above the surface; the C atom lies 1.11 Å above the surface. From the thermodynamic pathway for methane dissociation on the Cu(111) planar surface, shown in Fig. 6, clearly the dissociation of methane on this surface is highly unfavorable, with each step in the dissociation process costing more energy. In total, 87 kcal/mol is needed to go from CH_4 in the gas phase to separately adsorbed C and H atoms. This same pathway was calculated to cost 148 kcal/mol in a DFT cluster calculation published by Au et al. [30]. This difference is attributable to the different geometries (cluster vs slab) adopted in the calculations, leading to the smaller adsorption energies (by 5–10 kcal/mol) calculated within the cluster approach (shown in Table 1). All of the evidence indicates that the interaction of CH_x ($x = 0, \ldots, 3$) and H in general is far weaker on the Cu surface than that on the Ni(111) surface, where the same dissociation process for methane would cost only 8 kcal/mol (see Fig. 4).

3.2.2. *Cu(211) stepped surface*

Given that the (211) stepped surface has been found to be more reactive for Ni [18] and for other surfaces [37], it is important to consider methane dissociation on the Cu(211) stepped surface as well. Toward this end, we have calculated the adsorption energies of CH_x and H at the high symmetry sites of the Cu(211) surface, along with the transition states in the methane dissociation process. The adsorption energies are shown in Table 2. Again, all of the adsorbates lie at approximately the same positions on the Cu(211) surface as on the Ni(211) surface, and the adsorption energies at the preferred sites are lower than the corresponding energies on the Ni(211) surface. Transition states were also determined and are shown in Fig. 7. On the Cu(211) stepped surface, CH_4 dissociates at the 1f-edge position, with CH_3 adsorbing at the 2f-edge position and H initially moving to the 3f@1f-edge position. At the transition state, the C–H separation is 2.0 Å, and the barrier height is 33 kcal/mol. CH_3 adsorbs at the top of the step edge and tilts out over the step

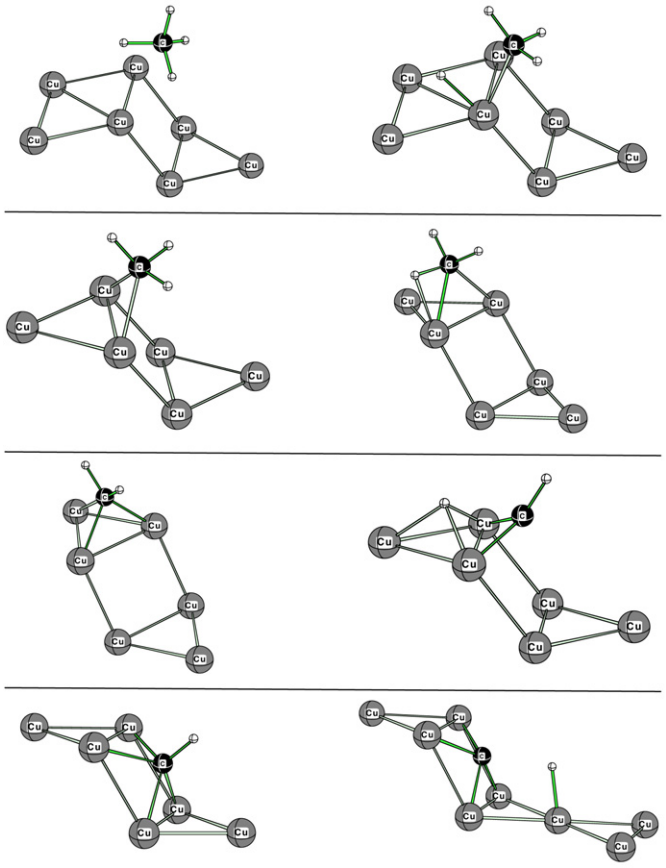

Fig. 7. Adsorption geometries of CH_x (on the left) and transition states (on the right) in the methane dissociation pathway on the Cu(211) stepped surface.

itself. The C–H bond length is 1.11 Å, and the H–C–H bond angles range from 103 to 109.5°. This variation in bond angles is caused by a distortion in the shape of CH_3 fragment through the interaction of one of the hydrogen atoms with a copper atom at the step edge. (The other two hydrogen atoms are rotated away from the copper atoms and do not experience a similar direct interaction with a surface copper atom.) The C–H bond is longer for the hydrogen atom closest to a surface copper atom (1.12 Å) than for the other two hydrogen atoms. It is this hydrogen atom that is most easily dissociated into the 3f@1f-edge position across the nearby copper atom. The C–H bond is stretched to 1.18 Å at the transition state with a reaction barrier of 32 kcal/mol. The resulting CH_2 fragment moves away from the step to the 3f@2f-edge position on the terrace. On the terrace site at the top of the step, CH_2 adopts much the same structure as that seen on the (111) surface, with one H atom pointing toward a copper atom and the other lying over the 2f-edge position. The C-Cu distances are 2.35 and 1.96 Å, with the carbon atom lying 1.96 Å from both edge copper atoms. Both C–H bonds have a length of 1.11 Å. Not surprisingly, the adsorption energy of 77 kcal/mol in the 3f@2f-edge position is very close to that seen on the Cu(111) surface, where CH_2 has an adsorption energy of 80 kcal/mol at the 3f position and 77 kcal/mol at the 2f position. CH_2 dissociates by moving out over the step and leaving the far hydrogen behind on the terrace in the 3f@2f-edge position. This C–H bond-breaking is the most expensive on the Cu(211) surface, costing 44 kcal/mol, with the C–H bond stretched to 1.86 Å at the transition state. After the C–H bond is broken, the CH fragment continues to move past the step edge and down into the 5f position in the face of the step. The hydrogen atom, as on the (111) surface, points straight out from the step face 1.11 Å above the carbon atom. The C–Cu distance is 2.00 Å from the step edge atoms and 2.01 Å from the step base atoms. From this 5f position, the hydrogen atom can move out over the nearest copper atom at the base of the step into the far 3f@2f-edge position (with the periodicity of the structure ensuring this site is at the top of the next step), leaving behind the carbon atom on the step face in the 5f position. This last step has a barrier of 42 kcal/mol, and the C–H bond has a length of 2.09 Å at the transition state. The hydrogen atom prefers to adsorb on the terrace at the 3f@2f-edge site with an adsorption energy of 60 kcal/mol. Much like in the case of CH_2, the adsorption geometry and energy are almost identical to those on the (111) surface where the adsorption energy for H is 56 kcal/mol at the 3f position. The remaining carbon atom experiences its strongest interaction with the Cu(211) surface on the face of the step and lies only 0.52 Å above the copper surface (compared with 1.11 Å above the Cu(111) surface) with a C–Cu distance of 1.88 Å. In contrast to hydrogen, the adsorption energy is increased dramatically to 134 kcal/mol on the step from 104 kcal/mol on the planar surface, but still lies well below the adsorption energies of C on either of the Ni planar (154 kcal/mol) or stepped (180 kcal/mol) surfaces. Although the Cu(211) stepped surface is found to be more reactive than the Cu(111) planar surface, the dissociation of methane is still endothermic, costing 48 kcal/mol. From these results, it is clear that carbon cokes will not form on copper surfaces, and that the activity of copper catalysts in the dissociation of methane will be very poor. These findings account for the lack of coking and for the poor activity of copper catalysts that has been observed experimentally in SOFC systems [5,57,59,66–72,90,91,93].

3.2.3. *Copper surface alloys*

Many experimental studies have been done on the Ni–Cu alloy system, in which it is believed that the alloy surface is Cu-enriched [5,65,69,71–73]. Despite this surface enrichment, Ni–Cu alloys still show activity for hydrocarbon dissociation and are susceptible to the formation of carbon cokes, even at Cu:Ni ratios of 9:1. It is important to note that this carbon formation on Cu–Ni alloys appears to be self-limiting and does not lead to fracture of the anode as is the case for nickel anodes [71]. Gorte et al. [71,72] noted that carbon formation is dependent on the temperature at which the anode is reduced in H_2. When the anode is reduced at temperatures above 800 °C, carbon deposition is greatly decreased. This could suggest increased enrichment of the surface with copper, along with blocking of the nickel step edges, or a more uniform mixing of the copper and nickel, because stabilization of graphitic carbon on the surface may require a minimum nickel ensemble size [18,41,96]. Given that Cu–Ni alloys still show relatively high activity, even for large Cu:Ni ratios, it is pertinent to ask whether this activity is due solely to exposed Ni particles on the surface or whether it might also be due to an increase in the activity of the surface copper

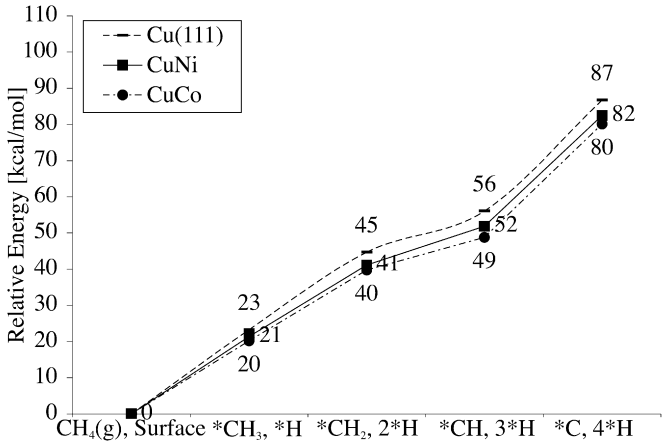

Fig. 8. Thermodynamic pathways for methane dissociation on Cu(111), on a copper–nickel(111) surface alloy and on a copper–cobalt(111) surface alloy. It is apparent that the underlying Ni and Co atoms have little effect on the binding properties of the copper monolayer.

due to interactions with the underlying nickel. Recent studies have suggested that surface or near-surface alloys can have dramatically different chemical properties than either of their constituent metals [96–99]. To answer this question, we have calculated the thermodynamic pathway for methane dissociation on a Cu–Ni surface alloy with a Cu(111) monolayer on top of a three-layer Ni(111) slab. The layer of copper and the top layer of nickel were first relaxed before adsorption energies were calculated. The results of this calculation, shown in Fig. 8, clearly show that the underlying nickel has little effect on the catalytic properties of the copper monolayer. All adsorbates are found to prefer the same 3f sites, and the adsorption energies are little changed from their values on a pure Cu(111) slab. Cobalt, along with nickel, is known to be a good reforming catalyst [5], and theoretical studies have shown Co to be an active catalyst for methane hydrogenation/dehydrogenation [28,29,47]. Whereas copper and nickel are miscible and form a bulk alloy, copper and cobalt are not miscible and will phase-segregate with copper coating the surface of the alloy [72,100]. An experimental study of Cu–Ni and Cu–Co alloys by Lee et al. [72] has shown that much less carbon will form on Cu–Co alloys and that Cu covers more of the Co surface than the Ni surface. A small increase in performance (about 20%) is observed on the addition of Co to the Cu-ceria anode, and this anode is stable against coke formation over several hours of operation. To model this Cu–Co alloy, we placed a monolayer of copper on top of three layers of cobalt placed in bulk-truncated positions in an fcc lattice with a lattice constant of $a_0 = 3.544$ Å. Cobalt is known to have a hexagonal closely packed structure, which changes to an fcc structure above 390 °C [101,102]. Because SOFCs operate at temperatures above 600 °C, we chose to use the fcc structure for Co. As was done for the Cu–Ni alloy, the layer of copper and the top layer of cobalt were allowed to relax before adsorption energies were calculated. Fig. 8 shows that this surface alloy of Cu–Co is only marginally more active than the Cu(111) surface and the Cu–Ni alloy, and that the Cu–Co surface alloy will do little to catalyze the dissociation of methane and the formation of graphitic carbon. This result suggests that the small gain in performance observed in SOFCs based on Cu–Co alloys [72] is likely due to small, exposed clusters of Co on the alloy surface, and that the resistance to coking is due to predominant coverage of the surface by Cu.

3.3. Blocking of the active step sites on Ni(211)

As discussed in Section 3.1, the dissociation of methane into carbon and four hydrogen atoms on the nickel surface is exothermic when carbon is able to adsorb at the step sites on the Ni(211) surface, but is endothermic on the Ni(111) surface. Theoretical and experimental studies have shown that carbon formation is nucleated at the step edges, followed by the growth of a graphene plane from the step edge covering the adjacent terrace sites [18,36,39]. The blocking of these active step sites by surface alloys or by promoter atoms has been proposed as a mechanism for discouraging carbon formation on Ni anodes [18,21]. In this section, we consider the effects of step-blocking in Cu–Ni alloys along with the effects of adding sulfur and gold promoter atoms to the Ni(211) surface.

3.3.1. Copper blocking nickel steps

As mentioned in Section 3.2.3, the surface of Cu–Ni alloys tends to be enriched with copper, because copper has a lower surface energy than nickel [5,65,69,71–73]. The results of a theoretical study of disordered bimetallic clusters by Zhu and DePristo [73] suggest that copper atoms will segregate to the surface and surround exposed Ni(111) islands, occupying all of the step and edge sites. Given that copper-enriched surfaces show evidence of regions of exposed nickel through their increased activity, along with a greater tolerance to coking (especially when reduced at higher temperatures [71,72]), it seems likely that the nickel steps that nucleate carbon formation are being blocked by copper atoms while the exposed terrace nickel sites are contributing to catalytic activity. We modeled this step-blocking by adding Cu atoms along the step edge of the Ni(211) surface, as shown in Fig. 9. The nickel atoms were kept frozen at their bulk-truncated positions, and the geometry of the copper atoms was allowed to relax. The positions of the copper atoms were then frozen, and the adsorption energies were calculated at the high-symmetry sites of the Cu–Ni(211) surface; results are given in Table 3. CH_3 adsorbs at the 2f-edge position, as it does on the Cu(211) and Ni(211) surfaces. The C–H bond lengths vary between 1.10 and 1.12 Å, and H–C–H bond angles range from 103° to 109.8°. The CH_3 fragment interacts primarily with two copper atoms on the step edge, and, not surprisingly, it has the same structure seen on Cu(211) in Fig. 7. The adsorption energy of 40 kcal/mol is almost identical to that on the Cu(211) surface of 41 kcal/mol. CH_2 sits at the 3f@2f-edge position, interacting directly with two copper atoms and one nickel atom. Its adsorption energy of 79 kcal/mol is only slightly larger than that on the Cu(211) surface of 77 kcal/mol. The interaction with the nickel atom seems to pull the carbon atom closer to the surface with a C–Ni distance of 2.20 Å and C–Cu distances of 1.94 Å. On the Cu(211) surface, these same distances are 2.35 Å from the terrace Cu atom and 1.96 Å from the step-edge copper atoms. Note that CH_2 sits just out of the

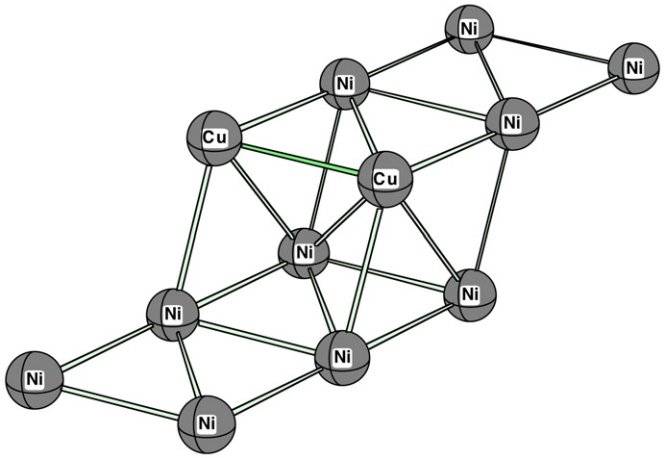

Fig. 9. Copper blocking the step edge on the Ni(211) surface.

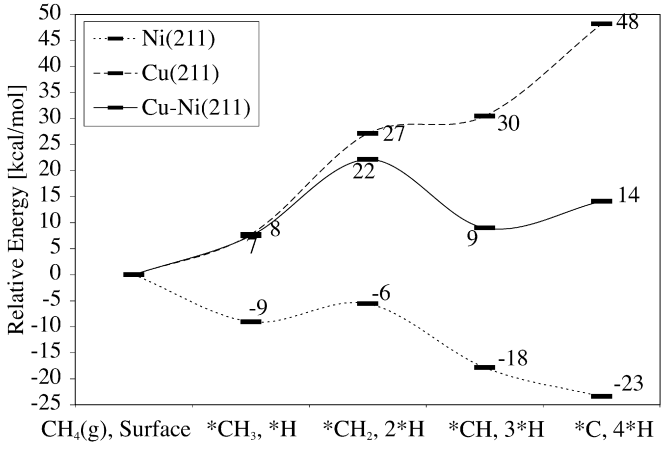

Fig. 10. Methane dissociation energies on the Ni(211) surface with the step edges blocked by Cu. The energy pathway follows that of Cu(211) in the first two steps before dipping to lower values.

Table 3
Adsorption energies of CH_x $(x = 0, \ldots, 3)$ and H at the preferred adsorption sites on the Cu–Ni(211) stepped surface

Adsorbate	Site	E_{ads} [kcal/mol]
H	3f@2f-edge	61
C	5f	162
CH	5f	143
CH_2	3f@2f-edge	79
CH_3	2f-edge	40

3f position, closer to the Cu atoms on the step edge than to the Ni atom. At the 5f position, CH has a much stronger interaction with the Cu–Ni(211) surface than with the Cu(211) surface, and the adsorption energy increases by 17 kcal/mol over its value on the Cu(211) surface (but is still 10 kcal/mol less than that on the Ni(211) surface). The C–H bond length is 1.11 Å, the C–Cu distance is 2.09 Å, and the C–Ni distances from the nearest base and terrace Ni atoms are 1.9 and 2.50 Å, respectively. We also calculated the transition state for dehydrogenation of CH and found a reaction barrier of 23 kcal/mol at a C–H bond length of 2.03 Å. In an earlier study [18], the same reaction barrier was calculated to be ∼19 kcal/mol on Ni(211). Given that the hydrogen atom dissociates across the nearest nickel atom, it is not surprising that the reaction barrier to CH dissociation is closer to its value on Ni(211) than on Cu(211), where it is 43 kcal/mol. Carbon sits at the 5f position as well, with an adsorption energy 28 kcal/mol greater than that on Cu(211) and 18 kcal/mol less than that on Ni(211). The C–Ni distance is 1.79 Å, and the C–Cu distance is 1.91 Å. Finally, hydrogen, which adsorbs at the 3f@2f-edge position, has an adsorption energy closest to its value on Cu(211), because it interacts with two copper atoms and one nickel atom. In all cases, the adsorption energies lie between their values on the Cu(211) and the Ni(211) surfaces. For those adsorbates, C and CH, which interact with a larger number of nickel atoms, the adsorption energies are closer to those on the Ni(211) surface. For those adsorbates that interact with a larger number of Cu atoms on the step edge, the adsorption energies are very close to those on the Cu(211) surface. The fact that the copper atoms lie along the step edge seems to increase the strength of their interaction with the adsorbates. This correspondence is seen in the thermodynamics of methane dissociation, shown in Fig. 10. For the first two steps in the path, dissociation of $CH_4(g) \rightarrow {}^*CH_3 + {}^*H$ and ${}^*CH_3 + {}^*H \rightarrow {}^*CH_2 + 2{}^*H$, the energies follow those of the Cu(211) surface. For the last two steps to ${}^*CH + 3{}^*H$ and ${}^*C + 4{}^*H$, the energies drop to values between those of the Cu(211) and Ni(211) surfaces. At an energy cost of 14 kcal/mol, methane dissociation is much more likely to occur on the Cu–Ni(211) surface than on the Cu(211) surface. The production of carbon is endothermic, however, and is much less likely to occur on this surface than on the Ni(211) surface. These results suggest that blocking of the Ni(211) step sites in Cu–Ni alloys is sufficient to suppress the formation of carbon cokes in SOFC anodes, while still allowing for high enough activity in the dissociation of methane.

3.3.2. Gold blocking nickel steps

Nickel and gold do not form a bulk alloy, but they have been shown to form a surface alloy with a mixture of gold and nickel atoms in the first atomic layer [96,103]. Because gold has an extended electron density, it is able to lower the nickel surface energy by increasing the effective coordination number of adjacent nickel atoms. Alloyed gold atoms have been shown to have a dramatic effect on the chemical properties of the Ni surface. Calculations by Kratzer et al. [16] have shown that the barrier to methane dissociation is increased by 4 and 9 kcal/mol on top of a Ni atom adjacent to one or two gold atoms, respectively. Whereas the barrier to methane dissociation is raised on the Ni–Au surface alloy, the adsorption of carbon has been shown to be completely destabilized on the Ni(111) surface at all 3f sites adjacent to a Au atom [96]. This observation that the effect of Au on carbon adsorption is much greater than its effect on methane dissociation was experimentally confirmed in a study (reported along with the above theoretical results in the same paper [96]) of the steam-reforming reaction on Ni and Au–Ni catalysts, in which the Au-containing sample was shown to resist carbon formation under conditions that led to poisoning of Ni catalysts. This resistance to the formation of graphitic carbon was argued to be a result of a reduction in the size of the average ensemble

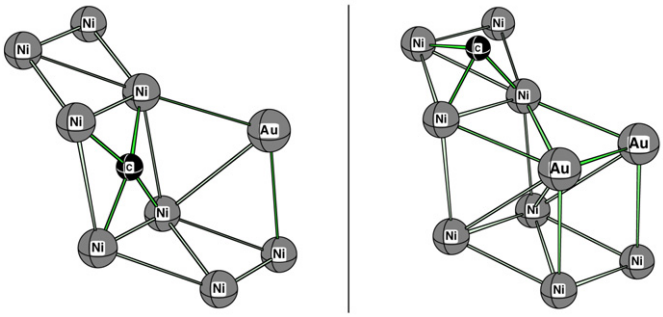

Fig. 11. Adsorption sites for carbon on the Ni(211) stepped surface with 50% (on the left) and 100% (on the right) of the step sites blocked by Au.

of nickel atoms due to the deactivation by Au of a large number of 3f sites. (Each Au atom would deactivate six adjacent 3f adsorption sites.) It is also likely that Au atoms would preferentially move to step sites on the Ni(211) surface, where Ni atoms would experience even lower coordination than in the Ni(111) terraces. Bengaard et al. [18] have shown that Au is more stable when it replaces a Ni atom at the step edge rather than one in a Ni(111) terrace, and that Au will segregate to the surface of a Au–Ni cluster with a preference for low-coordination sites. With this possibility in mind, we calculated the adsorption energies of CH_x ($x = 0, \ldots, 3$) and H on the Ni(211) surface with the steps partially and fully blocked by Au atoms. Interestingly, our calculations showed that Au is unable to block the adsorption of carbon at adjacent 5f sites (see Fig. 11) on the Ni(211) stepped surface when the Au step-blocking is at 50%, and that the dissociation of methane to carbon is exothermic. To prevent adsorption of carbon at the step sites of the Ni(211) surface, it is necessary to block 100% of the step sites with Au atoms. With 100% step-blocking, most of the adsorbates prefer to lie at the 3f position—surrounded by Ni atoms—away from the Au atoms at the step edge. CH_3 lies closer to the 2f-edge position than to the 3f@2f-edge position. This movement is caused by the repulsive interaction of one of the hydrogen atoms with a gold atom on the *previous* step. The adsorption energies (see Table 4) are within 5 kcal/mol of the adsorption energies on the Ni(111) planar surface. By blocking the step sites and repelling the adsorbates away from the step edges, the Au atoms force the adsorbates onto the Ni(111) terrace sites and prevent adsorption of carbon at the step edges.

3.3.3. *Sulfur-blocking nickel steps*

A number of studies of sulfur adsorption on Ni surfaces have shown that the addition of sulfur leads to both dramatic reductions in carbon formation and changes in the structure of the carbon adsorbed [18,21,41]. Rostrup-Nielsen [41] showed that high sulfur coverage leads to the formation of amorphous carbon rather than whisker carbon, and that sulfur is able to inhibit the rate of carbon formation more than it inhibits the rate of the steam-reforming reaction. Rostrup-Nielsen argued that ensembles of sulfur-free nickel atoms available on the surface were too small to allow for the nucleation of whisker carbon but large enough to catalyze the reforming reaction. However, STM studies [42] of sulfur coverage on Ni surfaces showed that islands of

Table 4
Adsorption energies at the preferred sites on the Au–Ni(211) surface with 100% Au step-blocking. The adsorption energy for carbon at the fivefold position on the Ni(211) surface with 50% Au step-blocking is also shown

Adsorbate	Site	E_{ads} [kcal/mol]
H	3f@2f-edge	63
C	3f@2f-edge	151
C (50% Au)	5f	168
CH	3f@2f-edge	139
CH_2	3f@2f-edge	88
CH_3	2f-edge	30

Table 5
Adsorption energies at the preferred sites on the Ni(211) surface with all step sites blocked by sulfur atoms

Adsorbate	Site	E_{ads} [kcal/mol]
H	3f@2f-edge	65
C	3f@2f-edge	143
CH	3f@2f-edge	134
CH_2	3f@2f-edge	79
CH_3	3f@2f-edge	34

sulfur atoms are nucleated at the step edges, and Bengaard et al. [18] have argued—based on detailed theoretical calculations—that the nucleation of graphitic carbon starts at the steps, with step-blocking playing a primary role in preventing carbon formation when small amounts of sulfur are added to Ni catalysts. Abild-Pedersen et al. [21], in a detailed experimental and theoretical examination of the effect of sulfur on carbon formation, have shown that the amount of deposited carbon drops rapidly with increasing sulfur coverage up to 0.06 S atoms/surface Ni atom, after which the effect of adding sulfur becomes much weaker. This coverage of 0.06 of a monolayer was shown to be in excellent agreement with the density of step sites on the Ni surface. Accompanying calculations showed that sulfur is more stable at the step sites on Ni(211) than on Ni(111). Although the barriers to the first step in the methane dissociation process—dehydrogenation of methane and co-adsorption of $^*CH_3$ and $^*H$—have been calculated for S–Ni(211) [21], the energy required to take the remaining steps in the methane dissociation pathway has yet to be calculated. We present here the first such calculations of the adsorption energies and transition states along the methane dissociation pathway from CH_4 to adsorbed $^*C + 4^*H$. To model the surface, nickel atoms are frozen in place at their bulk-truncated positions. Sulfur atoms are placed along the step edge of the Ni(211) surface and allowed to relax. The sulfur atoms are then frozen, and the adsorbate geometries are optimized and the adsorption energies calculated. As in the Au–Ni calculations discussed above, it is necessary to fully block the step with S to prevent adsorption of carbon at the step edge. The main results are thus reported for 100% coverage of the Ni(211) step edge by sulfur. Adsorption energies, given in Table 5, as in the case of Au–Ni (Table 4), are very close to the adsorption energies on the Ni(111) planar surface, although in the case of S–Ni, the adsorption energies are lower by ∼10 kcal/mol. This additional weakening of the interaction between the Ni surface and the adsorbates is likely due to the direct Pauli repulsion between the adsorbates and the sul-

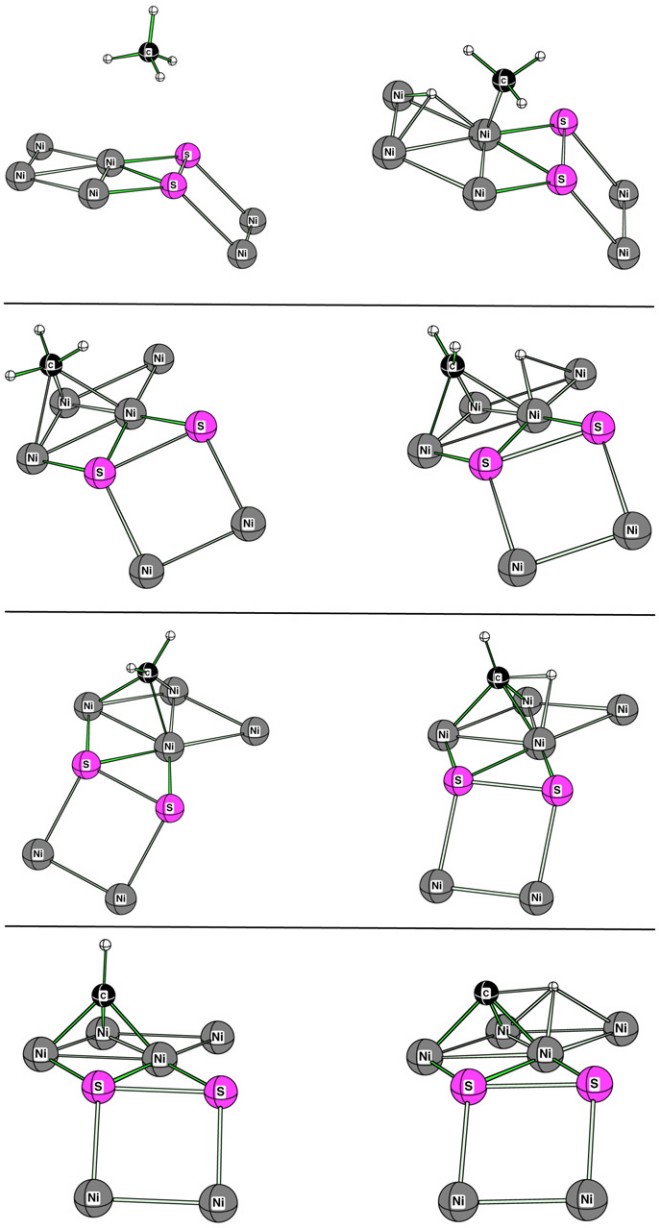

Fig. 12. Adsorption geometries for CH_x (on the left) and transition states (on the right) in the methane dissociation pathway on the on Ni(211) stepped surface with step sites blocked by sulfur atoms.

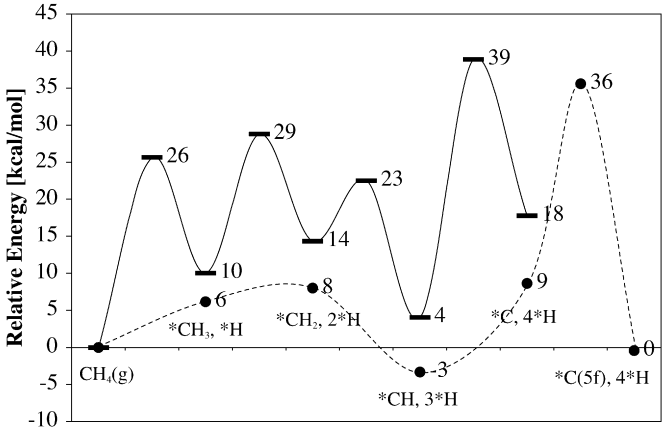

Fig. 13. Thermodynamic and kinetic barriers to methane dissociation on the Ni(211) stepped surface with steps blocked by sulfur atoms. The solid bars and line show the energies for the frozen surface and the circles and dashed line show the energies when the geometries of the surface Ni and S atoms are optimized, along with the barrier for C migration to the step site from the 3f@2f-edge site on the terrace.

fur atoms discussed in previous work [21,104]. All adsorbates were found to sit at the 3f@2f-edge position (see Fig. 12) surrounded by Ni atoms. The dissociation of methane starts at the 1f-edge position, with one of the hydrogen atoms dissociating into the 3f@1f-edge position. At the transition state, the C–H distance is 2.26 Å, and the C–Ni distance is 2.28 Å. The barrier to this initial dissociation is 26 kcal/mol, and $^*CH_3 + {}^*H$ has an energy 10 kcal/mol higher than $CH_4(g)$ + surface. This compares well with the values of 29 and 13 kcal/mol, respectively, calculated for the same process of methane dissociation at a 1f nickel site on Ni(211) with 50% step-blocking by Abild-Pedersen et al. [21]. CH_3 lies at a 3f@2f-edge position with all hydrogen atoms pointing toward the nearest three nickel atoms. The carbon atom is slightly closer to the step edge, and the C–H bonds in this direction are slightly longer than the C–H bond (1.12 vs at 1.11 Å), which points away from the step edge. The dissociation of CH_3 proceeds by the detachment of a hydrogen atom across a 2f bridge into the adjacent 3f@1f-edge position. The C–H bond stretches to 1.64 Å at the transition state, with a reaction barrier of 19 kcal/mol. The CH_2 fragment remains at the 3f@2f-edge position with one hydrogen atom pointing toward a Ni atom and the other pointing out over the 2f-edge position. Again, the hydrogen atom dissociates across a 2f bridge position into the adjacent 3f@1f-edge position with a C–H bond length of 1.25 Å at the transition state. The barrier to this step in the methane dissociation process is 8 kcal/mol. CH also remains at the 3f@2f-edge position with the hydrogen atom pointing straight up, perpendicular to the terrace. A tilt of the CH molecule is followed by dissociation of the hydrogen atom across the 2f bridge. The C–H bond length is stretched to 1.42 Å at the transition state, and the reaction barrier to this last step is a hefty 35 kcal/mol. From here, it is possible that the dissociated C atom in the 3f@2f-edge position might migrate to the 5f step position after first displacing the sulfur atom away from the step. To investigate this possibility, we repeated the above calculations of the adsorption sites and energies on the S–Ni(211) surface with optimization of the geometry of the (111) surface atoms of the nickel slab and of the sulfur atoms. Relaxation of the surface Ni atoms and S atoms enhances adsorption energies by 5 kcal/mol and does not qualitatively change the thermodynamic pathway (see Fig. 13). However, the adsorption energy of C can be further lowered by 8 kcal/mol from its value at the terrace 3f@2f-edge site if it is allowed to displace a sulfur atom away from the step edge. The transition state in this migration pathway, in which the sulfur atom is first pushed away from the step, costs 27 kcal/mol. Given that CH remains the most stable adsorbate and that there is a large barrier (35 kcal/mol) to the dissociation of CH on the terrace site (CH was not found to occupy the step site on the relaxed surface) and an additional barrier of 27 kcal/mol posed by the physical presence of the S atom to migration of the C atom from the terrace to the step

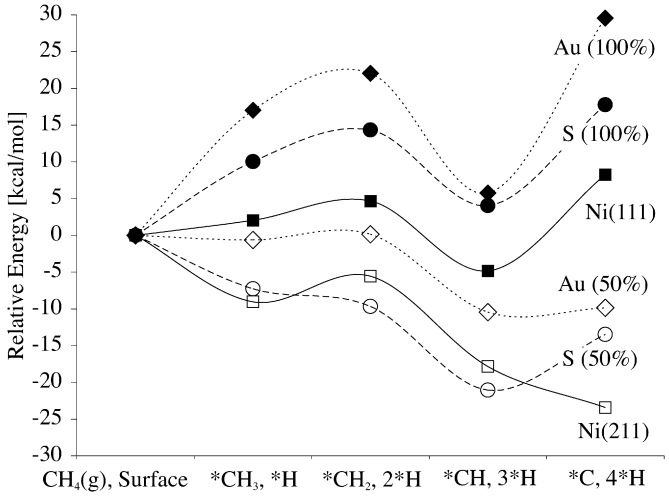

Fig. 14. Thermodynamic profile for methane dissociation on Ni(111) and Ni(211) (solid lines) compared to those for Au (dotted lines) and S (dashed lines) on Ni(211) with 50 and 100% blocking of the step edge sites.

site, it is safe to conclude that occupation of the 5f step sites by C is greatly hindered by the presence of sulfur. The full thermodynamic and kinetic pathway for methane dissociation on S–Ni with 100% step blocking is shown in Fig. 13. The reaction barriers to dehydrogenation on S–Ni(211) are comparable to those calculated for the Ni(111) surface by Bengaard et al. [18] (shown in Fig. 2). Along with the close agreement with the adsorption energies of Ni(111), this agreement in reaction barriers suggests that the interaction of the adsorbates with the Ni(211) surface with step sites blocked by sulfur atoms is dominated by the Ni(111) terraces lying between the step edges. This pattern is shown in Fig. 14, in which the thermodynamics of methane dissociation on the step-blocked Ni(211) surface is compared with that on the Ni(111) surface. With 50% step-blocking by either Au or S, the production of carbon at the step edge is exothermic. With 100% step-blocking, the dissociation of methane on Ni(211) mimics that on Ni(111), although the S and Au additives contribute to an additional repulsion and weaken the interaction of adsorbates with the terrace Ni atoms. In both cases, blocking of the step edge on Ni(211) prevents the adsorption of carbon on the step edge and hinders the nucleation of graphene from step edge sites. Further weakening of the interaction between the Ni atoms and the adsorbates will also frustrate the tendency to coking by reducing the area available to support the stable growth of graphene islands [18].

4. Conclusion

The propensity to coking shown by Ni catalysts can be explained by the strong adsorption of carbon atoms at the step sites on a Ni(211) surface, followed by the growth of graphitic carbon over the adjacent terrace sites [18,36,39]. The dissociation of methane to carbon and hydrogen is endothermic on the Ni(111) planar surface but is exothermic on the Ni(211) stepped surface. Copper has been observed to have low activity in SOFC systems and to be highly resistant to the formation of carbon cokes [5,57,59,71,90–93]. In agreement with these experimental findings, we have shown that the thermodynamic and kinetic barriers to methane dissociation are very high on both the Cu(111) planar and Cu(211) stepped surfaces. Although the step sites on Cu(211) are more active than the planar sites on Cu(111), as is the case for Ni, the dissociation of methane on Cu(211) remains highly endothermic. Studies of copper–nickel [5,65,69,71,72] and copper–cobalt [72] alloys have shown that the addition of copper can greatly reduce the amount of coking observed in SOFC systems, while still allowing the anode catalyst to retain some measure of activity. Our calculations of adsorption energies on Cu–Ni and Cu–Co surface alloys show that the underlying Ni or Co atoms have little effect on the chemical properties of the surface monolayer of Cu atoms. This implies that the activity observed in Cu–Ni and Cu–Co alloys is due to regions of exposed Ni or Co, and that the resistance to coking is due to Cu enrichment of the alloy surface and/or blocking of the active step sites [18,21]. Our calculations of adsorption energies on the Cu–Ni(211) alloy, in which the Ni(211) step sites are blocked by Cu atoms, show that the catalyst is able to retain a measure of activity, whereas the dissociation to separately adsorbed carbon and hydrogen atoms is shown to be endothermic. We have also considered, in some detail, the effects of blocking the Ni(211) step sites with Au and S promoter atoms. It has been shown that Au will form a surface alloy with Ni, and that the Au atoms will discourage coking more readily than they will discourage the reforming reaction [96]. Although large amounts of sulfur will poison a nickel catalyst, studies have shown that adding small amounts of sulfur will discourage coke formation [21,41], and that this sulfur is most likely to migrate to the step edges [18,21,42], where it will block the exothermic adsorption of carbon. Our calculations of the thermodynamics on Au–Ni(211) and S–Ni(211) show that step-blocking renders the step sites inactive to methane dissociation and forces adsorption of CH_x and H on the Ni(111) terrace sites. Our calculations of reaction barriers to dehydrogenation on S–Ni(211) are in good agreement with the methane dehydrogenation barrier calculated by Abild-Pedersen et al. [21] and very close to those calculated for the subsequent reaction steps on the sulfur-free Ni(111) planar surface by Bengaard et al. [18]. The calculations presented in this paper suggest that the observed reduction in coking in Cu–Ni, Au–Ni, and S–Ni catalysts is due to blocking of the active step sites on the nickel surface. We have shown that the activity of step-blocked Ni(211) is dominated by Ni(111) terraces, and that the formation of adsorbed carbon on step-blocked Ni(211) is endothermic. The additional effects of promoter atoms in repelling adsorbates and reducing the size of active Ni ensembles may also play a role. The residual coking observed in these systems is likely due to interactions of adsorbates with exposed Ni(111) terraces.

Acknowledgments

Financial support was provided by the Alberta Energy Research Institute and the Western Economic Diversification Department. All calculations were carried out on WestGrid computing resources, funded in part by the Canada Foundation for Innovation, Alberta Innovation and Science, BC Advanced Ed-

ucation, and the participating research institutions. The WestGrid equipment was provided by IBM, Hewlett Packard, and SGI.

References

[1] K. Joon, J. Power Sources 71 (1–2) (1998) 12–18.
[2] S.M. Haile, Mater. Today 6 (2003) 24–29.
[3] R.M. Ormerod, Chem. Soc. Rev. 32 (1) (2003) 17.
[4] A. Atkinson, S. Barnett, R.J. Gorte, J.T.S. Irvine, A.J. McEvoy, M. Mogensen, S.C. Singhal, J. Vohs, Nat. Mater. 3 (2004) 17.
[5] S. McIntosh, R.J. Gorte, Chem. Rev. 104 (2004) 4845.
[6] S.S.C. Chuang, Catalysis 18 (2005) 186–198.
[7] B. Johnston, M.C. Mayo, A. Khare, Technovation 25 (2005) 569.
[8] R.J. Kee, H. Zhu, D.G. Goodwin, Proc. Combust. Inst. 30 (2005) 2379.
[9] M.B. Lee, Q.Y. Yang, S.L. Tang, S.T. Ceyer, J. Chem. Phys. 85 (3) (1986) 1693–1694.
[10] T.P. Beebe Jr., D.W. Goodman, B.D. Kay, J.T. Yates Jr., J. Chem. Phys. 87 (4) (1987) 2305–2315.
[11] I. Chorkendorff, I. Alstrup, S. Ullmann, Surf. Sci. 227 (3) (1990) 291–296.
[12] B.Ø. Nielsen, A.C. Luntz, P.M. Holmblad, I. Chorkendorff, Catal. Lett. 32 (1–2) (1995) 15–30.
[13] Q.Y. Yang, K.J. Maynard, A.D. Johnson, S.T. Ceyer, J. Chem. Phys. 102 (19) (1995) 7734–7749.
[14] J.H. Larsen, I. Chorkendorff, Surf. Sci. Rep. 35 (5–8) (1999) 163–222.
[15] B. Hammer, J.K. Nørskov, Nature 376 (1995) 238.
[16] P. Kratzer, B. Hammer, J.K. Nørskov, J. Chem. Phys. 105 (1996) 5595–5604.
[17] R.M. Watwe, H.S. Bengaard, J.R. Rostrup-Nielsen, J.A. Dumesic, J.K. Nørskov, J. Catal. 189 (2000) 16–30.
[18] H.S. Bengaard, J.K. Nørskov, J. Sehested, B.S. Clausen, L.P. Nielsen, A.M. Molenbroek, J.R. Rostrup-Nielsen, J. Catal. 209 (2002) 365–384.
[19] J.R. Rostrup-Nielsen, J. Sehested, J.K. Nørskov, Adv. Catal. 47 (2002) 65–139.
[20] R.T. Vang, K. Honkala, S. Dahl, E.K. Vestergaard, J. Schnadt, E. Lægsgaard, B.S. Clausen, J.K. Nørskov, F. Besenbacher, Nat. Mater. 4 (2005) 160–162.
[21] F. Abild-Pedersen, O. Lytken, J. Engbæk, G. Nielsen, I. Chorkendorff, J.K. Nørskov, Surf. Sci. 590 (2005) 127–137.
[22] J. Schüle, P. Siegbahn, U. Wahlgren, J. Chem. Phys. 89 (11) (1988) 6982–6988.
[23] P.E.M. Siegbahn, I. Panas, Surf. Sci. 240 (1990) 37–49.
[24] O. Swang, K. Faegri Jr., O. Gropen, U. Wahlgren, P. Siegbahn, Chem. Phys. 156 (3) (1991) 379–386.
[25] H. Yang, J.L. Whitten, Surf. Sci. 255 (1991) 193–207.
[26] H. Yang, J.L. Whitten, J. Am. Chem. Soc. 113 (1991) 6442–6449.
[27] H. Yang, J.L. Whitten, J. Chem. Phys. 96 (1992) 5529–5537.
[28] H. Burghgraef, A.P.J. Jansen, R.A. van Santen, J. Chem. Phys. 101 (12) (1994) 11,012–11,020.
[29] H. Burghgraef, A.P.J. Jansen, R.A. van Santen, Surf. Sci. 324 (2–3) (1995) 345–356.
[30] C.-T. Au, M.-S. Liao, C.-F. Ng, J. Phys. Chem. A 102 (1998) 3959–3969.
[31] A. Michaelides, P. Hu, Surf. Sci. 437 (1999) 362–376.
[32] A. Michaelides, P. Hu, J. Chem. Phys. 112 (2000) 6006–6014.
[33] A. Michaelides, P. Hu, J. Chem. Phys. 112 (18) (2000) 8120–8125.
[34] R. Rosei, F. Ciccacci, R. Memeo, C. Mariani, L.S. Caputi, L. Papagno, J. Catal. 83 (1) (1983) 19–24.
[35] Y. Gamo, A. Nagashima, M. Wakabayashi, M. Terai, C. Oshima, Surf. Sci. 374 (1–3) (1997) 61–64.
[36] S. Helveg, C. López-Cartes, J. Sehested, P.L. Hansen, B.S. Clausen, J.R. Rostrup-Nielsen, F. Abild-Pedersen, J.K. Nørskov, Nature 427 (2004) 426–429.
[37] S. Dahl, A. Logadottir, R.C. Egeberg, J.H. Larsen, I. Chorkendorff, E. Törnqvist, J.K. Nørskov, Phys. Rev. Lett. 83 (1999) 1814–1817.
[38] J.K. Nørskov, T. Bligaard, A. Logadottir, S. Bahn, L.B. Hansen, M. Bollinger, H. Bengaard, B. Hammer, Z. Sljivancanin, M. Mavrikakis, Y. Xu, S. Dahl, C.J.H. Jacobsen, J. Catal. 209 (2) (2002) 275–278.
[39] F. Abild-Pedersen, J.K. Nørskov, J.R. Rostrup-Nielsen, J. Sehested, S. Helveg, Phys. Rev. B 73 (2006) 115419.
[40] P.M. Holmblad, J.H. Larsen, I. Chorkendorff, J. Chem. Phys. 104 (18) (1996) 7289–7295.
[41] J.R. Rostrup-Nielsen, J. Catal. 85 (1984) 31–43.
[42] V. Maurice, N. Kitakatsu, M. Siegers, P. Marcus, Surf. Sci. 373 (2–3) (1997) 307–317.
[43] S.T. Ceyer, Q.Y. Yang, M.B. Lee, J.D. Beckerle, A.D. Johnson, Stud. Surf. Sci. Catal. 36 (1988) 51.
[44] J.R. Rostrup-Nielsen, L.J. Christiansen, Appl. Catal. A 126 (2) (1995) 381–390.
[45] H.S. Bengaard, I. Alstrup, I. Chorkendorff, S. Ullmann, J.R. Rostrup-Nielsen, J.K. Nørskov, J. Catal. 187 (1) (1999) 238–244.
[46] J.J. Mortensen, B. Hammer, J.K. Nørskov, Surf. Sci. 414 (3) (1998) 315–329.
[47] X.-Q. Gong, R. Raval, P. Hu, J. Chem. Phys. 122 (2005) 024711.
[48] J.-F. Paul, P. Sautet, J. Phys. Chem. B 102 (9) (1998) 1578–1585.
[49] A. Michaelides, P. Hu, J. Am. Chem. Soc. 122 (40) (2000) 9866–9867.
[50] I.M. Ciobîcă, F. Frechard, R.A. van Santen, A.W. Kleyn, J. Hafner, J. Phys. Chem. B 104 (2000) 3364–3369.
[51] I.M. Ciobîcă, R.A. van Santen, J. Phys. Chem. B 106 (24) (2002) 6200–6205.
[52] C.T. Au, M.-S. Liao, C.-F. Ng, Chem. Phys. Lett. 267 (1997) 44–50.
[53] M.-S. Liao, C.-T. Au, C.-F. Ng, Chem. Phys. Lett. 272 (5–6) (1997) 445–452.
[54] C.-T. Au, C.-F. Ng, M.-S. Liao, J. Catal. 185 (1) (1999) 12–22.
[55] N. Kiratzis, P. Holtappels, C.E. Hatchwell, M. Mogensen, J. Irvine, Fuel Cells 1 (3–4) (2001) 211–218.
[56] R. Craciun, S. Park, R.J. Gorte, J.M. Vohs, C. Wang, W.L. Worrell, J. Electrochem. Soc. 146 (11) (1999) 4019–4022.
[57] S. Park, R. Craciun, J.M. Vohs, R.J. Gorte, J. Electrochem. Soc. 146 (1999) 3603–3605.
[58] R.J. Gorte, S. Park, J.M. Vohs, C. Wang, Adv. Mater. 12 (19) (2000) 1465–1469.
[59] S. Park, J.M. Vohs, R.J. Gorte, Nature 404 (2000) 265–267.
[60] H. Kim, S. Park, J.M. Vohs, R.J. Gorte, J. Electrochem. Soc. 148 (7) (2001) A693–A695.
[61] R.J. Gorte, H. Kim, J.M. Vohs, J. Power Sources 106 (1–2) (2002) 10–15.
[62] C. Lu, W.L. Worrell, R.J. Gorte, J.M. Vohs, J. Electrochem. Soc. 150 (3) (2003) A354–A358.
[63] A. Costa-Nunes, J.M. Vohs, R.J. Gorte, J. Electrochem. Soc. 150 (7) (2003) A858–A863.
[64] S. McIntosh, J.M. Vohs, R.J. Gorte, Electrochem. Solid State Lett. 6 (11) (2003) A240–A243.
[65] J.H. Sinfelt, J.L. Carter, D.J.C. Yates, J. Catal. 24 (1972) 283–296.
[66] C.A. Bernardo, I. Alstrup, J.R. Rostrup-Nielsen, J. Catal. 96 (1985) 517–534.
[67] N.M. Rodriguez, M.S. Kim, R.T.K. Baker, J. Catal. 140 (1993) 16–29.
[68] I. Alstrup, M. Tavares, C. Bernardo, O. Sørensen, J. Rostrup-Nielsen, M.T. Tavares, C.A. Bernardo, Mater. Corros. 49 (1998) 367–372.
[69] M. Tavares, I. Alstrup, C. Bernardo, Mater. Corros. 50 (1999) 681–685.
[70] T.V. Reshetenko, L.B. Avdeeva, Z.R. Ismagilov, A.L. Chuvilin, V.A. Ushakov, Appl. Catal. A 247 (2003) 51–63.
[71] H. Kim, C. Lu, W.L. Worrell, J.M. Vohs, R.J. Gorte, J. Electrochem. Soc. 149 (2002) A247–A250.
[72] S.-I. Lee, J.M. Vohs, R.J. Gorte, J. Electrochem. Soc. 151 (2004) A1319–A1323.
[73] L. Zhu, A.E. DePristo, J. Catal. 167 (1997) 400–407.
[74] G. Kresse, J. Hafner, Phys. Rev. B 48 (1993) 13,115–13,118.
[75] G. Kresse, J. Hafner, Phys. Rev. B 49 (20) (1994) 14,251–14,269.
[76] G. Kresse, J. Furthmüller, Comput. Mater. Sci. 6 (1996) 15–50.
[77] G. Kresse, J. Furthmüller, Phys. Rev. B 54 (1996) 11,169–11,186.
[78] P.E. Blöchl, Phys. Rev. B 50 (1994) 17,953–17,979.
[79] G. Kresse, D. Joubert, Phys. Rev. B 59 (1999) 1758–1775.
[80] J.P. Perdew, K. Burke, M. Ernzerhof, Phys. Rev. Lett. 77 (1996) 3865–3868.
[81] H.J. Monkhorst, J.D. Pack, Phys. Rev. B 13 (1976) 5188–5192.

[82] P. Villars, L.D. Calvert, Pearson's Handbook of Crystallographic Data for Intermetallic Phases, American Society of Metals, Metals Park, OH, 1985.
[83] H. Jónsson, G. Mills, K.W. Jacobsen, Nudged elastic band method for finding minimum energy paths of transitions, in: B.J. Berne, G. Ciccotti, D.F. Coker (Eds.), Classical and Quantum Dynamics in Condensed Matter Phase Simulations, World Scientific, Singapore, 1998, pp. 385–404.
[84] G. Henkelman, H. Jónsson, J. Chem. Phys. 113 (2000) 9978.
[85] G. Henkelman, B.P. Uberuaga, H. Jónsson, J. Chem. Phys. 133 (2000) 9901.
[86] J.P. Perdew, K. Burke, Y. Wang, Phys. Rev. B 54 (1996) 16,533.
[87] B. Hammer, L.B. Hansen, J.K. Nørskov, Phys. Rev. B 59 (1999) 7413.
[88] S. Kurth, J.P. Perdew, P. Blaha, Int. J. Quantum Chem. 75 (4–5) (1999) 889.
[89] M. Gajdoš, A. Eichler, J. Hafner, J. Phys. Condens. Matter 16 (2004) 1141.
[90] A. Frennet, G. Lienard, G. Verhaegen, J. Res. Inst. Catal. 16 (1) (1968) 115–153.
[91] A.I. La Cava, C.A. Bernardo, D.L. Trimm, Carbon 20 (3) (1982) 219.
[92] G.-C. Wang, J. Li, X.-F. Xu, R.-F. Li, J. Nakamura, J. Comput. Chem. 26 (2005) 871.
[93] S. Jung, M.D. Gross, R.J. Gorte, J.M. Vohs, J. Electrochem. Soc. 153 (8) (2006) A1539.
[94] A. Michaelides, P. Hu, J. Chem. Phys. 114 (2001) 2523.
[95] Z.-X. Chen, K.M. Neyman, K.H. Lim, N. Rosch, Langmuir 20 (2004) 8068.
[96] F. Besenbacher, I. Chorkendorff, B.S. Clausen, B. Hammer, A.M. Molenbroek, J.K. Nørskov, I. Stensgaard, Science 279 (1998) 1913.
[97] B. Hammer, M. Scheffler, Phys. Rev. Lett. 74 (1995) 3487.
[98] J. Greeley, M. Mavrikakis, Nat. Mater. 3 (2004) 810.
[99] J.R. Kitchin, J.K. Nørskov, M.A. Barteau, J.G. Chen, Phys. Rev. Lett. 93 (2004) 156801.
[100] S.-K. Kim, J.-S. Kim, J.Y. Han, J.M. Seo, C.K. Lee, S.C. Hong, Surf. Sci. 453 (1–3) (2000) 47–58.
[101] C.S. Barrett, T.B. Massalski, Structure of Metals, McGraw–Hill, New York, 1966.
[102] C.J. Smithells (Ed.), Metals Reference Book, fifth ed., Butterworth, Scarborough, ON, 1976.
[103] L.P. Nielsen, F. Besenbacher, I. Stensgaard, E. Lægsgaard, C. Engdahl, P. Stoltze, K.W. Jacobsen, J.K. Nørskov, Phys. Rev. Lett. 71 (1993) 754–757.
[104] F. Abild-Pedersen, J. Greeley, J.K. Nørskov, Catal. Lett. 105 (2005) 9.